1989 SPIE Symp. on Advances in Intelligent Robotics Systems, Nov. 1989, Philadelphia PA

MULTIRESOLUTIONAL SENSOR FUSION BY CONDUCTIVITY ANALYSIS

H.E.Stephanou and A.M.Erkmen
Center for Artificial Intelligence
School of Information Technology
George Mason University
Fairfax, Virginia 22030
stephano@gmuvax2.gmu.edu

Abstract

This paper describes an evidential pattern classifier for the combination of data from physically different sensors. We assume that the sensory evidence is multiresolutional, incomplete, imprecise, and possibly inconsistent. Our focus is on two types of sensory information patterns: visual and tactile. We develop a logical sensing scheme by using a model based representation of prototypical 3D surfaces. Each surface represents a class of topological patterns described by shape and curvature features. The sensory evidence is classified by using a *conductivity* measure to determine which prototypical surface best matches the evidence. A formal evidential model of uncertainty is used to derive logical sensors and provide performance measures for sensor integration algorithms.

1. INTRODUCTION

Robot sensing algorithms perform well for relatively complete and precise data and simple environments. Sensory information in realistic applications tends, however, to be simultaneously overconstrained (e.g. redundant data due to a higher level of resolution than required by the task) and underconstrained (sparse or incomplete data due to sensor limitations and/or occlusion). When prior knowledge about unstructured environments is incomplete, the procedural knowledge required for sensory data interpretation is generally specified in terms of *flexible* concepts [6] that have imprecise and context-dependent meaning.

For sensors of the same physical type, data fusion is generally performed at a *low* (signal) level. For physically different sensors, each type of sensor is modeled separately, processes and interprets its own data, then transmits its individual, sensor-dependent perception to a decentralized system. Global inferences made during sensory data interpretation require a common frame where *high* level data can be compared and processed. A task dependent, high level (knowledge based) model for sensor integration is therefore desirable. To maximize the modularity and reusability of sensor fusion systems, we opt for a slightly different approach where data fusion occurs at an *intermediate* (pattern) level. We consider sensory information *patterns* consisting of a set of sensor and task independent features.

Section 2 of this paper is a brief review of a previously developed evidential classifier for multiresolutional patterns. This classifier is then applied to shape features extracted from visual data (section 3) and curvature features extracted from tactile data (section 4). In section 5, results from these two steps are combined to generate information patterns in a common frame of topological surfaces.

2. EVIDENTIAL PATTERN CLASSIFICATION

This section reviews the evidential classifier described in [3]. The presentation is rather qualitative, in an attempt to highlight the underlying concepts. Mathematical details may be found in [3].

2.1 Evidential patterns

Our approach to pattern classification is based on the theory of belief functions [7]. Belief functions are particularly well suited for the representation of evidential patterns in which some features may be missing, or where the data supports some coarse statement about a set of features, rather than a more refined statement about individual features. Bayesian methods assume a complete probabilistic model. Rather than completing the model, the DS theory computes provability or plausibility indices.

2.2 Information fractals

Regular sets have exact topology and their size is measured as an integer dimension. The size and density of irregular sets, on the other hand, can only be estimated. This estimation is performed by the canonical measure of a regular set and yields a fractional dimension. Fractal sets have two basic properties: (i) their boundary is broken into fine irregularities, (ii) they include gaps, which makes their density irregular. Similarly, information patterns can be deformed into fine irregularities, or they can have heterogeneous density due to the existence of information gaps. Information patterns may consist of signal patterns, such as a set of irregular image edges. Or they may consist of knowledge patterns, such as a set of prototypical belief functions with information gaps between focal elements. We call such patterns *information fractals*.

2.3 Entropy of a belief function

We use the concept of entropy as a measure of uncertainty within as well as between the focal elements of a belief function. Entropy [3,9] provides a useful and convenient characterization of information *gaps*, or cavities. These information gaps are at the basis of our fractal characterization of belief functions. They can be characterized by two types of distances: (i) distances between elements of a set (equivalent to the concept of *size* of a set); and (ii) distances between sets. The larger these distances are, the more they break the information *compactness* of the belief function. Under total certainty, the belief function is totally compact, the focal elements shrink to points, and the interset distances are zero. The *volume* of a belief function is viewed as a set of fractional dimension. As the level of certainty is increased (through active sensing for example), the belief functions become more *compact*, the information gaps shrink, and their dimensions tend to integral values, thus reducing their fractal characteristic.

2.4 Fractal dimension of a belief function

A fractal is defined as a scale invariant structure whose statistical properties are unchanged under dilation or change of spatial length scale. Our approach is based on fractal sets of fractional dimension [4]. This *dimension* is a measure of the *size* of the set. The more nearly a fractal object fills a Euclidean space of integral dimension n, the closer its dimension approaches n. The fractal dimension provides an estimate of the spread of a fractal set. The fractal representation of a belief function is based on the specification of its *fractal dimension*. The dimension conveys information about the distribution of uncertainty within the focal elements as well as between them. *Vacuum* in a physical system loosens its structure, thus increasing entropy. Similarly, gaps between the focal elements of a belief function cause the loosening of the information structure due to uncertainty, and are measured by the value of entropy.

2.5 Conductivity of a belief function

The evidential classifier relies on a knowledge base that includes a set of prototypical rules. The antecedent of each rule consists of observable features (modeled as belief functions), while the consequent is one of the decision classes, or hypotheses [8]. The design of the evidential classifier requires the analysis of the *interaction* between a belief function representing some observed sensory evidence, and the aggregate of prototypical belief functions representing the rule antecedents. The strength of the interaction provides a measure of the *conductivity*, or relevance of the knowledge aggregate to the evidence input. Conductivity is caused by the one-to-one interaction between the input and each belief function in the aggregate.

3. LOGICAL SHAPE SENSING

In this section we develop a logical shape sensing algorithm that uses an evidential classifier [3] to (i) extract high level shape features from segmented images, and (ii) assign belief values to those features. This is done through a three-level process as shown in fig. 1.

3.1 Edge fitting

The first level of the logical sensor deals with *edge fitting*. The input is a set of disjoint *edge segments* obtained from an edge detector. We assume that edge linking has been applied to clusters of edge segments. Link-lists are used, so these edges are ordered. The set of all edge segments and link-edges (fig. 2) is approximated by a *fitted edge* with end points x and y.

The belief assigned to fitted edges depends on several sources of error due to occlusion, noise, insufficient resolution, and inaccuracies in edge detection algorithms. The belief assigned to the fitted edge is:

$$b_{xy} = \frac{|x-y|}{L(\Gamma)}(1-\sin\Phi)\frac{n^*}{n^\Gamma}$$

where $L(\Gamma)$ is the sum of the lengths of the edge segments and link-edges, n^* is the number of edge segments with this angle, and n^Γ is the total number of edge segments and link-edges. $\frac{|x-y|}{L(\Gamma)}$ is the approximation error of the length measure. Φ is the smallest acute angle between the detected edge segments and the fitted line. Its contribution to the belief assignment is $1-\sin\Phi$.

A belief of $(1-b_{xy})$ is assigned to the frame of discernment, and reflects the uncertainty about the edge fitting process.

3.2 Primitive formation

The second level maps the geometric evidence extracted by the edge-fitting level into incomplete topological *shape primitives* such as **rectangle, square, triangle**. Shape primitives express geometric constraints between two or more edges. The output of this level is a belief function with singleton focal elements that correspond to each shape primitive. The belief assigned to a shape primitive is heuristically determined by the closeness of its match to prototypical shape primitives.

3.2.1 The rectangle primitive

We consider five sources of error for matching a set of geometrical fitted edge attributes to the rectangle primitive: (i)opposite sides of the hypothesized rectangle do not have exactly the same length; (ii)opposite sides are not exactly parallel; (iii)adjacent sides are not exactly perpendicular; (iv)some sides are missing; and (v)some sides are not connected. The belief assigned to the rectangle from its topological attributes is:

$$b_{rectangle} = \frac{1}{4}(b_{AB}+b_{BC}+b_{CD}+b_{DA})\cdot$$

$$\frac{\min(|AB|,|CD|)}{\max(|AB|,|CD|)}\cdot\frac{\min(|BC|,|AD|)}{\max(|BC|,|AD|)}\cdot$$

$$|\sin\angle ABC|\cdot|\sin\angle BCD|\cdot|\sin\angle CDA|\cdot|\sin\angle DAB|$$

The first term attenuates the belief for a rectangular pattern when sides in the pattern are missing. The second term attenuates the belief when opposite sides are not equal. The third term attenuates the belief when opposite sides are not parallel. The first two terms also attenuate belief when adjacent sides are not connected.

3.2.2 The square primitive

The errors in matching a pattern of fitted edges geometry to the square primitive include those described above for the rectangle, in addition to the constraint that all sides must have equal length. The belief associated with the construction of a square is:

$$b_{square} = \frac{1}{16}(b_{AB}+b_{BC}+b_{CD}+b_{DA})$$

$$\left(\frac{\min(|AB|,|BC|)}{\max(|AB|,|BC|)}+\frac{\min(|BC|,|CD|)}{\max(|BC|,|CD|)}+\right.$$

$$\left.\frac{\min(|CD|,|DA|)}{\max(|CD|,|DA|)}+\frac{\min(|DA|,|AB|)}{\max(|DA|,|AB|)}\right)$$

$$|\sin\angle ABC|\cdot|\sin\angle BCD|\cdot|\sin\angle CDA|\cdot|\sin\angle DAB|$$

The addition (rather than multiplication as in the case of the rectangle) of min-max terms increases the sensitivity of the belief value to missing edges.

3.2.3 The triangle primitive

The topological constraints imposed on a triangle are more relaxed than those imposed on a rectangle or square, since : (i) fewer sides are required for its construction, (ii) there are no length or parallelism constraints on the sides, and (iii) the only angle constraints is summation to 2π. The belief assigned to the construction of a triangle is:

$$b_{triangle} = \frac{1}{3}(b_{AB} + b_{BC} + b_{CA})(1 - |\sin(\angle ABC + \angle BCA + \angle CAB)|)$$

3.3 Feature extraction

In the previous section, incomplete patterns of fitted edge data were classified into primitive shapes such as rectangle (R), square (S), triangle (T), circle (C), and bracket (B). The construction of the last two primitives was omitted for the sake of brevity. This classification is primarily based on geometric attributes, and may result in substantial ambiguity when the data are sparse. In the third and final level of the logical sensor, we define a broader set of classes, called *shape features*, that rely on the more robust topological attributes of the fitted edge patterns. Each class of shape features is characterized by a non-exhaustive set of prototypical shape features. The input belief function from the second level is classified (using the evidential classifier) into one of the following features: **Rectangular, Triangular, Elliptical.**

The three classes used for the above example are listed in table 1. Each feature class is represented by an aggregate of prototypes. The class of rectangular features has a single prototype, $\Gamma_R^S = \{R_1\}$. The classes of triangular and elliptical features have two prototypes each: $\Gamma_T^S = \{T_1, T_2\}$ and $\Gamma_E^S = \{E_1, E_2\}$.

Class 1 abstracts lower level classes of rectangle and square primitives into a higher level class labeled Rectangular features. In this class, the topological relationship between a rectangle and a square (a special type of rectangle) is recognized. Class 2 abstracts triangular and elliptical primitives into a higher level class of Triangular features. Finally, class 3 recognizes that circles and c-shaped brackets are special cases of ellipses, and are therefore abstracted into an Elliptical features class. Focal elements in the prototypes reflect topological confusion between the constituent singletons. The beliefs assigned to each focal element are determined during a training period, and depend on the frequency of occurrence of the focal elements. $F_p^s = \cup(R, S, T, E, C, B)$ denotes the shape primitive frame of discernment.

Table 1 - Shape features

Class	Label	Prototypes
Γ_R^s	Rectangular	$R_1 = [\{R, S, (R, S)\}:\{0.2, 0.2, 0.6\}]$
Γ_T^s	Triangular	$T_1 = [\{T, E, (T, E), F_p^s\}:\{0.4, 0.1, 0.3, 0.2\}]$ $T_2 = [\{T, (T, S), F_p^s\}:\{0.5, 0.4, 0.1\}]$
Γ_E^s	Elliptical	$E_1 = [\{E, B, (E, C, B)\}:\{0.2, 0.1, 0.7\}]$ $E_2 = [\{E, B, F_p^s\}:\{0.5, 0.4, 0.1\}]$

3.4 Example

Fig. 3 illustrates an example of the edge-fitting and belief assignment procedure. Three clusters of edge segments are approximated by three fitted lines: AB, BC, and CD.

Edge fitting generates three simple support functions:

$E_1 = [\{AB, F^s_p\}; \{0.31, 0.69\}]$

$E_2 = [\{BC, F^s_p\}; \{0.15, 0.85\}]$

$E_3 = [\{CD, F^s_p\}; \{0.15, 0.85\}]$

Assuming that $\angle ABC = 80°$ and $\angle BCD = 100°$, the belief function assigned to the shape primitives is:

$X^s_p = [\{rectangle, square, triangle, F^s_p\}; \{0.19, 0.10, 0.20, 0.51\}]$

This is the output of the shape primitive formation level.

Applying the evidential classifier to this belief function yields the conductivities:

$\sigma^*(X^s_p, \Gamma^s_R) = 0.48$ for the class of rectangular features,

$\sigma^*(X^s_p, \Gamma^s_T) = 1.46$ for the class of triangular features, and

$\sigma^*(X^s_p, \Gamma^s_E) = 0$ for the class of elliptical features.

The conductivity value reflects the interaction of the input belief function with each of the prototypes. The interaction of the input with a given aggregate is large if the aggregate is well structured, i.e. if it includes a large number of belief functions. In the above example, although the input evidence was found to have high interaction dimension with Γ^s_R, its conductivity in this class is low. This is due to the fact that Γ^s_R has a single belief function, and is therefore considered ill-structured.

Normalizing the values of the conductivities in the shape feature frame of discernment F^S_f yields the shape feature belief function: $X^s_f = [\{\Gamma^s_R, \Gamma^s_T\}; \{0.25, 0.75\}]$

In summary, the logical shape sensor extracts high level topological shape features by progressively abstracting low level geometric information about image edges. It also uses a systematic procedure for the assignment of belief to the shape features.

4. LOGICAL CURVATURE SENSING

In this section we derive a logical curvature sensor aimed at complementing the shape sensor introduced in the previous paper. The rolling of a hard curved fingertip on a stationary surface is modeled as a logical touch sensor. We first develop an exploratory finger rolling strategy for the extraction of curvature features of 3D surfaces.

4.1 Local curvature estimation by finger rolling

We consider a tactile sensor consisting of an array of pressure sensitive cells, and attached on a rigid, spherical section of the fingertip (fig. 4). The local curvature of some unknown surface is to be estimated by rolling the fingertip against it.

For a finger rolling about a fixed point O on a planar surface, the apex C of the conical section sweeps a spherical surface $\Xi(t)$ centered at O, and of radius a.

4.1.1 Fingertip envelope

We assume that C is constrained to the surface $\Xi(t)$. Then, the rolling fingertip sweeps a family of spheres of radius a, and centered on $\Xi(t)$. The *sensing envelope* $\Psi(t)$ to this family of spheres is defined as a surface which is tangent at each point to one of the spheres (fig.4), and such that in every neighborhood of the point of contact with a surface there are points of contact with other spheres from the family. During the rolling motion, cells of the fingertip array are activated by the pressure due to contact with the surface being explored.

4.1.2 Cone signature

During a rolling motion of the fingertip, ϕ is held constant, while θ is varied. $\Xi(t)$ then becomes a planar curve. At every point of the curve, the *Frenet* frame consists of three unit vectors: (i) the tangent τ, the principal normal n, and the binormal vector $b = \tau \times n$. A directional frame is used, such that $n^{\cdot} = \epsilon n$ where $\epsilon = \pm 1$ depending on whether $\Xi(t)$ is concave upward or concave downward.

The curvature of the cone signature in $\Xi(t)$ when the finger is rolled on a perfectly planar surface is:

$$K_{cone} = -\frac{|\dot{r} \times \ddot{r}|}{|\dot{r}|^3} = -\frac{1}{a}$$

where $r = [x \; y \; z]^T$.

Since the fingertip is assumed to be spherical, its curvature is:

$$K_{tip} = \frac{1}{a}$$

The curvature of the fingertip envelope $\Psi(t)$ is:

$$K_{envelope} = \frac{1}{2a}$$

Let $\zeta(t)$ be some surface that is in contact with the finger, and let K_ζ denote the unknown local curvature of that surface at the point of contact. The three curvatures are related by: $K_\zeta = K_{cone} - K_{tip}$ where K_{cone} is the estimated curvature of the measured cone signature.

4.1.3 Tactile point spread function

When the fingertip contacts a rigid surface, an ideal tactile array would be activated at the contact point only. We assume that the tactile array has finite resolution, i.e. several cells are activated according to some point spread function. Fig. 5 shows a point $Q \in \Psi(t)$ in the neighborhood of the contact point $P \in \Psi(t)$. We now examine several sources of error introduced by this effect.

4.1.4 Local curvature belief assignment

We consider an exploratory finger rolling procedure where the finger is rolled along several meridian planes defined by $\phi_1, \ldots, \phi_{m_\phi}$. Let $P_{i1}, \ldots, P_{im_\theta}$ be the contact points during the rolling motion along the ith meridian plane $(1 \le i \le m_\phi)$. These points occur for $\theta = \theta_{i1}, \ldots, \theta_{im_\theta}$. We denote the normal pressure at each contact by: $\tau_{i1}, \ldots, \tau_{im_\theta}$. The point Q_{ij} is located at $(\phi_i + \Delta\phi_k, \theta_j + \Delta\theta_k)$ on the sensing envelope, and will be called the kth *neighbor* $(1 \le k \le N)$ of the contact point P_{ij}. v_{ijk} denotes the pressure recorded by a cell located at Q_{ijk}. d_{ijk} is the distance between Q_{ijk} and the plane tangent to the sensing envelope at P_{ij}. The curvature K_{cone_i} of the cone signature in the ith meridian plane can be computed from the angular position of the distal finger joint. The belief assigned to K_{cone_i} is:

$$b_i = \frac{|1 + aK_{cone_i}|}{\sum_{j=1}^{m_\theta} \tau_{ij}} \sum_{j=1}^{m_\theta} \left(\frac{\tau_{ij} - \sum_{k=1}^{N} v_{ijk} d_{ijk}}{\sum_{k=1}^{N} d_{ijk}} \right)$$

$|1 + aK_{cone_i}|$ is the value of the estimated curvature. When it is small, the belief is reduced since the accuracy of the approximation degrades. The second term discounts the belief assigned to the curvature by an amount proportional to the *smearing* of the tactile array. No discounting occurs when a single cell comes in contact with the sensed surface. The product $v_{ijk} d_{ijk}$ discounts the belief when large pressures are measured at cells that are distant from the sensing surface.

4.2 Primitive formation

We consider the following set of *curvature primitives*: planar (P), cylindrical down (C-), cylindrical up (C+), hyperbolic (H), elliptical down (E-), and elliptical up (E+) (fig. 6).

The curvature primitives frame of discernment: $F_p^c = \{P, C-, C+, H, E-, E+\}$ is defined in table 3, where γ is a small positive number corresponding to the minimum curvature threshold. A curvature primitive is defined as *planar* if the estimated curvatures along all rolling directions and at all rolling sites are such that: $0 \le K_{\xi_i} \le \gamma \ , \forall i$. Similarly, the curvature primitive is defined as *cylindrical up* if all the estimated curvatures are positive, and some of them exceed the threshold, while others are below it. The belief assigned to each of the curvature primitives is obtained by averaging the beliefs assigned to the estimated local curvatures K_{ξ_i} that support that curvature primitive. Averaging is performed over all rolling directions and sites.

Table 3 - Curvature primitive

Curvature primitive	Symbol	$\exists K_{\xi_i}$		
Planar	P	$-\gamma \le K_{\xi_i} \le \gamma$		
Cylindrical up	C+	$\gamma < K_{\xi_i}$	$-\gamma \le K_{\xi_j} \le \gamma$	
Cylindrical down	C-	$-\gamma \le K_{\xi_i} \le \gamma$	$K_{\xi_j} < -\gamma$	
Elliptical up	E+	$\gamma < K_{\xi_i}$	$\gamma < K_{\xi_j}$	
Elliptical down	E-	$K_{\xi_i} < -\gamma$	$K_{\xi_j} < -\gamma$	
Hyperbolic	H	$\gamma < K_{\xi_i}$	$-\gamma \le K_{\xi_i} \le \gamma$	$K_{\xi_j} < -\gamma$

4.3 Feature extraction

The evidential classifier is applied to the curvature primitives into one of three classes of curvature features. These classes correspond to quasiplanar, curved, and occluded surfaces, respectively, as determined from a combination of shape and curvature primitives: (i) the set of shape primitives, namely: rectangle (R), triangle (T), ellipses (E), brackets (B) and circles (C), and (ii) a disjoint set of curvature primitives (fig. 6) that includes the following elements: planar (P), cylindrical down (C-), cylindrical up (C+), hyperbolic (H), elliptical down (E-), elliptical up (E+), and no contact (N). The curvature primitive frame of discernment is:

$F_f^c = (R, T, E, B, C) \cup (P, C-, C+, H, E-, E+, N)$

This selection of curvatures features is useful for the detection of holes and cavities corresponding to occluded surfaces, i.e. for surfaces over which contact occurs at sites not belonging to surfaces that have undergone shape analysis. The curvature feature frame of discernment is: $F_f^c = \{Q, K, O\}$. Table 4 lists prototypes for each of the feature classes. We represent each feature class by an aggregate of two prototypes. For example, the class of quasiplanar features is represented by: $\Gamma_Q^c = \{Q_1, Q_2\}$

The feature classes reflect prior knowledge about the association between region shape primitives extracted from vision data and curvature shape primitives extracted from touch data. Each prototype contains information about the frequency of association between a given shape and curvature. The prototypes in the class of quasiplanar surfaces indicate that rectangular shape primitives are frequently associated with planar curvature primitives.

Prototype K_1 in the class of curved surfaces indicates that Rectangular and Triangular shape primitives are often associated with cylindrical curvature primitives. Similarly, K_2 indicates that Ellipse and Circle shape primitives are associated with elliptical up or elliptical down curvature primitives.

The prototypes in the class of occluded surfaces correspond to situations where vision data are gathered over a region around the opening of a hole or cavity while finger rolling occurs at over an occluded surface such as the bottom of the cavity or the walls of a hole. Curvature primitives and shape primitives are therefore extracted over different surfaces. This is denoted by the symbol N ("no contact") in table 4.

Table 4 - Curvature features

Class	Label	Prototypes
Γ_Q^c	Quasiplanar	$Q_1 = [\{(R,P),(R,(C-,C+)),(R,(H,C-,C+)),F_j^c\};\{0.5,0.3,0.1,0.1\})$ $Q_2 = [\{((R,T),P),F_j^c\};\{0.7,0.3\}]$
Γ_C^c	Curved	$K_1 = [\{((T,R),(C-,C+)),(B,E-),F_j^c\};\{0.5,0.4,0.1\}]$ $K_2 = [\{((E,C),(E-,E+)),F_j^c\};\{0.7,0.3\}]$
Γ_O^c	Occluded	$O_1 = [\{((R,T,S),(P,C-,C+),N),((E,B,C),(P,C-,C+),N),F_j^c\};\{0.7,0.2,0.1\}]$ $O_2 = [\{((E,B,C),(E-,E+,H),N),F_j^c\};\{0.7,0.3\}]$ $O_3 = [\{((R,T,S),P,N),F_j^c\};\{0.8,0.2\}]$ $O_4 = [\{((E,C),(P,E-,E+),N),F_j^c\};\{0.9,0.1\}]$

To assign belief to each of the curvature features classes, we compute the conductivity of the curvature primitive belief function into each one of the classes, then normalize the results.

4.4 Example

The logical sensing scheme was simulated for a simple example involving two rolling sites, with four meridian directions per site. Table 5 lists, for each of the eight cases, the estimated local curvature and the belief assigned to it. An "X" in the column of a primitive curvature indicates that the estimated curvature supports this curvature primitive. The belief b_i assigned to the local curvature is used in the computation of the total belief assigned to the curvature primitive. The balance of the belief is assigned to the curvature frame of discernment. The last row shows the total belief assigned to each of the primitive curvatures.

The output of the curvature primitive formation level is the belief function:

$X_p^c = [\{P, C-, C+, H\};\{0.10, 0.25, 0.28, 0.37\}]$

Applying the evidential classifier to this belief function yields the conductivities:

$\sigma^c(X_p^c, \Gamma_Q^c) = 1.30,\ \sigma^c(X_p^c, \Gamma_K^c) = 0,\ \sigma^c(X_p^c, \Gamma_O^c) = 0$

for the classes of planar, curved, and occluded features, respectively. These results indicate that the tactile evidence supports planar surfaces only, since contact has occurred, and the estimated local curvatures are small.

Table 5 - Curvature belief assignments

	ϕ	K_{t_i}	b_i	P	C-	C+	H
Site 1	0°	0.2	0.15	x		x	
	30°	0.1	0.07	x		x	
	90°	0.8	0.56			x	
	150°	0.1	0.08	x		x	
Site 2	0°	0.0	0.00	x	x	x	x
	30°	1.0	0.67			x	x
	80°	0.2	0.20	x	x	x	
	150°	-1.0	0.67		x		x
Belief				0.10	0.25	0.28	0.37

5. COMBINATION OF SHAPE AND CURVATURE EVIDENCE

The fusion of shape and curvature data is accomplished by combining the outputs of the shape and curvature feature extraction levels. The procedure is illustrated by extending the numerical examples from sections 3.4 and 4.4.

5.1 Shape and curvature classification

For this example, the conductivities of shape and curvature primitives in their respective feature classes are summarized below:

Shape

$\sigma^s(X_p^s, \Gamma_R^s) = 0.48 \quad \sigma^s(X_p^s, \Gamma_T^s) = 1.46 \quad \sigma^s(X_p^s, \Gamma_E^s) = 0$

for the classes of rectangular, triangular, and elliptical features, respectively.

Curvature

$\sigma^c(X_p^c, \Gamma_Q^c) = 1.30 \quad \sigma^c(X_p^c, \Gamma_K^c) = 0 \quad \sigma^c(X_p^c, \Gamma_O^c) = 0$

for the classes of planar, curved, and occluded features, respectively.

5.2 Curvature from shape

To combine the tactile and visual sensory evidence, we first compute the conductivity of the shape features X_j^s in each of the curvature feature classes.

Quasiplanar features: conductivity of X_j^s in Γ_Q^c requires that at least one of the prototypes in that class be *activated*. The activation of prototype Q_1 requires support for R, while the activation of Q_2 requires support for (R,T). The conductivity of the visual evidence in Γ_Q^c is therefore:

$\sigma^s(X_j^s, \Gamma_Q^c) = \max\{\sigma^s(X_p^s, \Gamma_R^s); \sigma^s(X_p^s, \Gamma_R^s) \cdot \sigma^s(X_p^s, \Gamma_T^s)\} = 0.48$

Curved features: the activation of prototype K_1 requires support for (T,R), while the activation of K_2 requires support for (E,C). The conductivity of X_j^s in Γ_K^c is therefore:

$$\sigma^s(X_j^s, \Gamma_K^c) = \max\{\sigma^s(X_p^s, \Gamma_T^s) \cdot \sigma^s(X_p^s, \Gamma_R^s); \sigma^s(X_p^s, \Gamma_B^s); \sigma^s(X_p^s, \Gamma_E^s) \cdot \sigma^s(X_p^s, \Gamma_C^s)\}$$

$$= \max\{1.46 \times 0.48; 0; 0\} = 0.70$$

Occluded features: a similar analysis for the class of occluded surfaces yields:

$$\sigma^s(X_j^s, \Gamma_O^c) = 0$$

5.3 Fusion of shape and curvature patterns

Since conductivity is a measure, it is additive. For the purposes of sensor fusion, we consider the conductivity of sensory patterns into the curvature feature frame as the sum of two conductivities:

$$\sigma^{c \wedge s}(\Gamma_i^c) = \sigma^c(X_p^c, \Gamma_i^c) + \sigma^s(X_j^s, \Gamma_i^c)$$

$\sigma^c(X_p^c, \Gamma_i^c)$ and $\sigma^s(X_j^s, \Gamma_i^c)$ respectively denote the conductivity of the curvature primitives (from touch data) and shape features (from vision data) in the Ith curvature feature class.

The total (combined) conductivities are obtained by simple addition:

$$\sigma^{c \wedge s}(\Gamma_Q^c) = \sigma^c(X_p^c, \Gamma_Q^c) + \sigma^s(X_j^s, \Gamma_Q^c) = 1.78$$

$$\sigma^{c \wedge s}(\Gamma_K^c) = \sigma^c(X_p^c, \Gamma_K^c) + \sigma^s(X_j^s, \Gamma_K^c) = 0.70$$

$$\sigma^{c \wedge s}(\Gamma_O^c) = \sigma^c(X_p^c, \Gamma_O^c) + \sigma^s(X_j^s, \Gamma_O^c) = 0$$

Normalization is finally performed to yield the combined curvature feature belief function:

$$X_j^c = [\{\Gamma_Q, \Gamma_K, \Gamma_O\}; \{0.72, 0.28, 0\}]$$

6. CONCLUSIONS

The evidential classification of information patterns from multiple disparate sensors is considered in this paper. We assume that the sensory evidence is multiresolutional, incomplete, imprecise, and possibly inconsistent. Our focus is on two types of sensory information patterns: visual and tactile. A logical sensor was developed by using a model based representation of prototypical 3D surfaces. Each surface represents a class of topological patterns described by shape and curvature features. Sensory patterns are classified by using a *conductivity* measure to determine which prototypical surface best matches the evidence.

We are currently extending the techniques described in this paper along three main directions: (i) the recognition of 3D objects in a robot manipulation environment, and (ii) the development of active sensing strategies to sequentially acquire the most relevant data at the appropriate level of resolution, and (iii) the incorporation of the sensor data fusion techniques into algorithms for sensorimotor control of multifingered robot hands. By using our fractal model of belief functions, we derive a measure of interframe capacity that allows the projection of uncertain sensory evidence among incompatible (and task dependent) frames of discernment, corresponding to different sensor, object and grasp models.

7. ACKNOWLEDGMENTS

This research was conducted in the Center for Artificial Intelligence at George Mason University. Research activities of the Center are supported in part by Defense Advanced Research Projects Agency under grant, administered by the Office of Naval Research, No. N00014-87-K-0874, in part by the Office of Naval Research under grant No. N00014-88-K-0226, and in part by the Office of Naval Research under grant No. N00014-88-K-0397.

8. REFERENCES

1. P.K.Allen, "Integrating vision and touch for object recognition tasks," *Int. J. Robotics Research*, Vol.7, No.6, pp.15-33, 1988.
2. H.F.Durrant-Whyte, "Sensor models and multisensor data," *Int. J. Robotics Research*, Vol.7, No.6, pp.97-113, 1988.
3. A.M.Erkmen and H.E.Stephanou, "Information fractals for an evidential classifier," *Proc. IEEE Int. Symposium on Intelligent Control*, 1988.

4. K.J.Falconer, *The geometry of fractal sets*, Cambridge University Press, 1985.
5. T.C.Henderson and C.Hansen, "The specification of distributed sensing and control," *J. Robotic Systems*, Vol. 2, pp. 387-396, 1985.
6. R.S.Michalski, I.Mozetic, J.Hong, and N.Lavrac, "The multipurpose incremental learning system AQ15 and its testing application to three medical domains," *Proc. 5th AAAI*, pp. 1041-1045, 1986.
7. G.Shafer, *A Mathematical Theory of Evidence*, Princeton Press, 1976.
8. H.E.Stephanou and A.M.Erkmen, "Evidential classification of dexterous grasps for the integration of perception and action," *Journal of Robotic Systems*, Vol.5, No.4, pp.309-336, 1988.
9. H.E.Stephanou and S.Y.Lu, "Measuring consensus effectiveness by a generalized entropy criterion," *IEEE Trans. Pattern Analysis and Machine Intelligence*, Vol. 10, No.4, pp.544-554, 1988.
10. H.E.Stephanou and A.M.Erkmen, "Shape and curvature data fusion by conductivity analysis," in *Multisensor Fusion for Computer Vision*, J.K.Aggarwal, Ed., NATO ASI Series, Springer-Verlag, to appear, 1990.

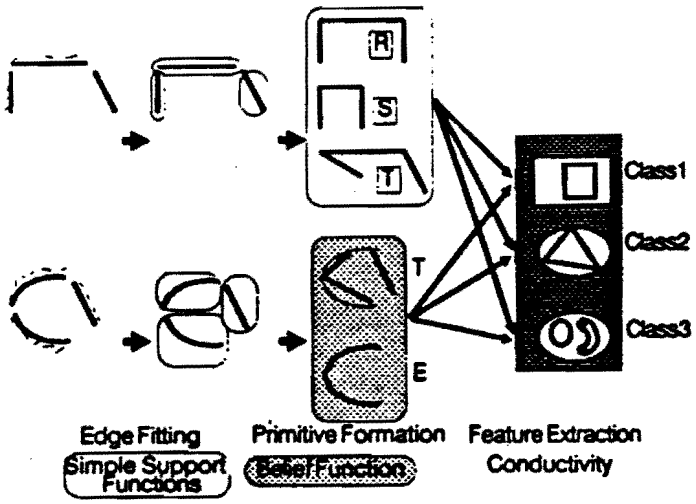

Fig. 1 Multilevel shape sensing

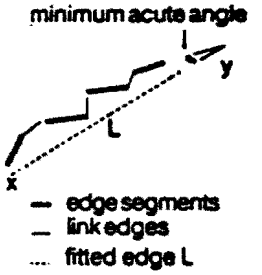

Fig. 2 Edge fitting

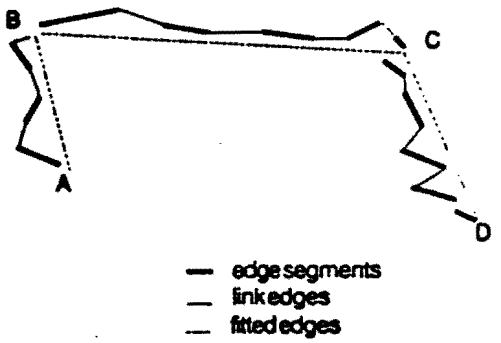

Fig. 3 Fitting the edges of a rectangle

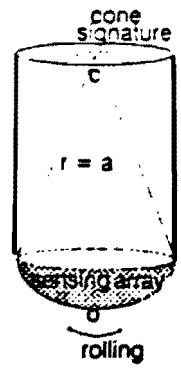

Fig. 4a Tactile sensor

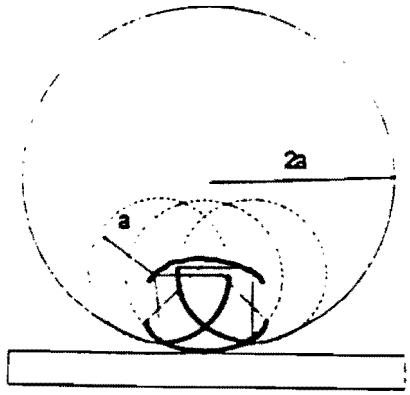

Fig. 4b Sensing envelope

Fig. 4 Finger rolling

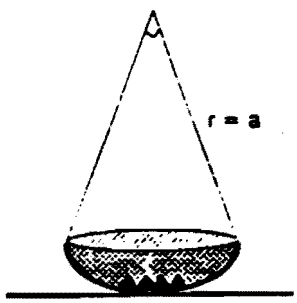

Fig. 5a activated neighbors in smeared contact

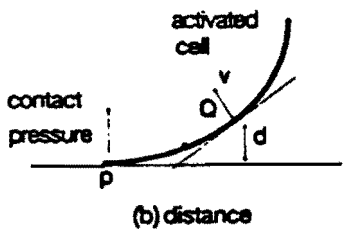

Fig. 5b distance

Fig. 5 Contact neighborhood

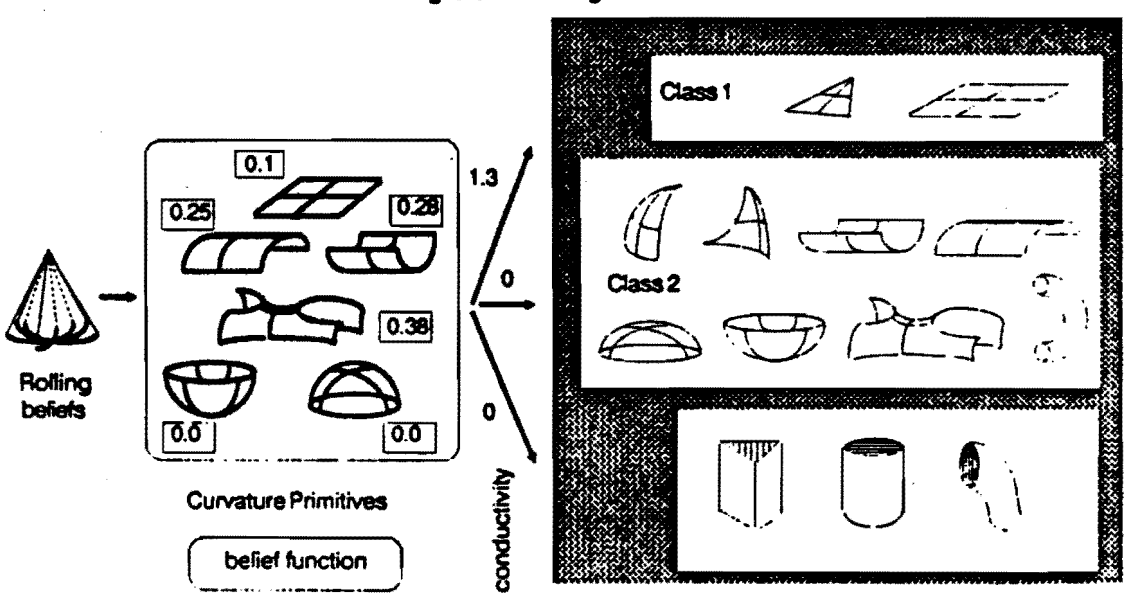

Fig. 6 Multilevel curvature sensing

4. K.J.Falconer, *The geometry of fractal sets*, Cambridge University Press, 1985.
5. T.C.Henderson and C.Hansen, "The specification of distributed sensing and control," *J. Robotic Systems*, Vol. 2, pp. 387-396, 1985.
6. R.S.Michalski, I.Mozetic, J.Hong, and N.Lavrac, "The multipurpose incremental learning system AQ15 and its testing application to three medical domains," *Proc. 5th AAAI*, pp. 1041-1045, 1986.
7. G.Shafer, *A Mathematical Theory of Evidence*, Princeton Press, 1976.
8. H.E.Stephanou and A.M.Erkmen, "Evidential classification of dexterous grasps for the integration of perception and action," *Journal of Robotic Systems*, Vol.5, No.4, pp.309-336, 1988.
9. H.E.Stephanou and S.Y.Lu, "Measuring consensus effectiveness by a generalized entropy criterion," *IEEE Trans. Pattern Analysis and Machine Intelligence*, Vol. 10, No.4, pp.544-554, 1988.
10. H.E.Stephanou and A.M.Erkmen, "Shape and curvature data fusion by conductivity analysis," in *Multisensor Fusion for Computer Vision*, J.K.Aggarwal, Ed., NATO ASI Series, Springer-Verlag, to appear, 1990.

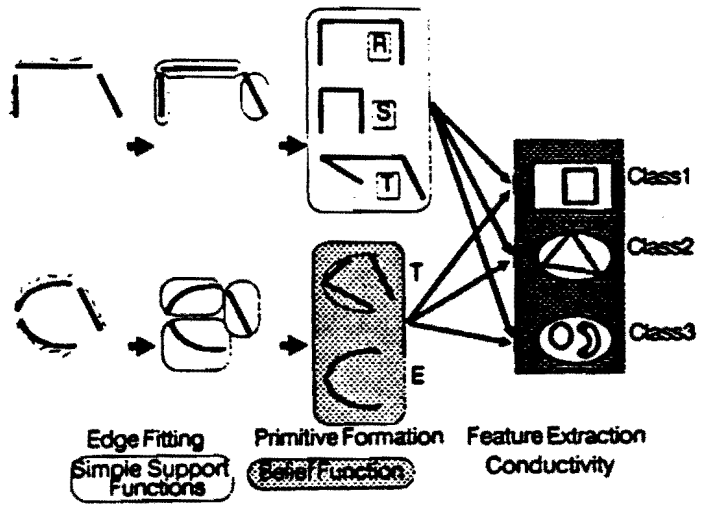

Fig. 1 Multilevel shape sensing

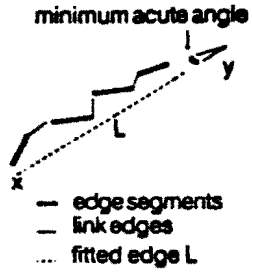

Fig. 2 Edge fitting

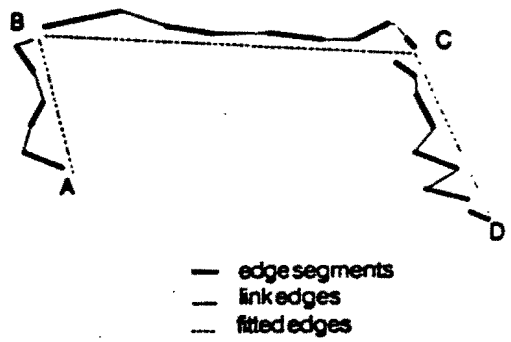

Fig. 3 Fitting the edges of a rectangle